The Journal of Chemical Physics ARTICLE pubs.aip.org/aip/jcp

Atomic scale structure and bond stretching force constants in stoichiometric and off-stoichiometric kesterites

Cite as: J. Chem. Phys. 159, 154705 (2023); doi: 10.1063/5.0169755
Submitted: 28 July 2023 • Accepted: 29 September 2023 •
Published Online: 19 October 2023

Konrad Ritter,[1,2,a)] Galina Gurieva,[3] Stefanie Eckner,[1,2] René Schwiddessen,[3] Francesco d'Acapito,[4] Edmund Welter,[5] Susan Schorr,[3,6] and Claudia S. Schnohr[1,2]

AFFILIATIONS

[1] Felix-Bloch-Institut für Festkörperphysik, Universität Leipzig, Linnéstraße 5, 04103 Leipzig, Germany
[2] Institut für Festkörperphysik, Friedrich-Schiller-Universität Jena, Max-Wien-Platz 1, 07743 Jena, Germany
[3] Helmholtz-Zentrum Berlin für Materialien und Energie, Hahn-Meitner-Platz 1, 14109 Berlin, Germany
[4] CNR-IOM-OGG c/o ESRF, 71 Avenue des Martyrs, 38000 Grenoble, France
[5] Deutsches Elektronen-Synchrotron DESY, Notkestr. 85, 22607 Hamburg, Germany
[6] Institut für Geologische Wissenschaften, Freie Universität Berlin, Malteserstr. 74-100, 12249 Berlin, Germany

[a)] **Author to whom correspondence should be addressed:** konrad.ritter@physik.uni-leipzig.de

ABSTRACT

The deviation from stoichiometry and the understanding of its consequences are key factors for the application of kesterites as solar cell absorbers. Therefore, this study investigates the local atomic structure of off-stoichiometric Cu_2ZnSnS_4 (CZTS), $Cu_2ZnSnSe_4$ (CZTSe) and $Cu_2ZnGeSe_4$ (CZGSe) by means of Extended X-ray Absorption Fine Structure Spectroscopy. Temperature dependent measurements yield the bond stretching force constants of all cation-anion bonds in stoichiometric CZTS and CZTSe and nearly stoichiometric CZGSe. Low temperature measurements allow high precision analysis of the influence of off-stoichiometry on the element specific average bond lengths and their variances. The overall comparison between the materials is in excellent agreement with measures like ionic/atomic radii and bond ionicities. Furthermore, the small uncertainties allow the identification of systematic trends in the Cu–Se and Zn–Se bond lengths of CZTSe and CZGSe. These trends are discussed in context of the types and concentrations of certain point defects, which gives insight into the possible local configurations and their influence on the average structural parameters. The findings complement the understanding of the effect of off-stoichiometry on the local structure of kesterites, which affects their electronic properties and thus their application for solar cells.

I. INTRODUCTION

Kesterite type materials, often just referred to as kesterites, are a group of materials that in their basic form are made up of at least four elements in a I_2–II–IV–VI_4 composition. These materials are promising for application as absorbers in both photovoltaics and photochemistry.[1,2] Their main advantages in any of the possible applications are the abundance of the required elements and the stability of the resulting solids. Typically the used elements are also non-toxic and not amongst the critical raw materials as defined by politics e.g. the European Commission.[3] The most common kesterites are Cu_2ZnSnS_4 (CZTS) and $Cu_2ZnSnSe_4$ (CZTSe), but any of the elements in these materials has also been replaced by suitable candidates in a multitude of studies.[4]

In their ability to convert sunlight into electrical power the main disadvantage of kesterites is evident in their conversion efficiency of 12.7%.[4–6] The difference between this record and the theoretical limit of around 30%[7] is mostly attributed to a low open circuit voltage present in devices throughout the literature.[1,2] The root cause of the low efficiency as compared to other solar cell

absorber materials, however, is still under debate. All high performance devices share a deviation from the original stoichiometry towards a Cu poor and Zn rich regime. While it was proven that these compounds usually still adopt the kesterite structure,[8] their compositional deviations cause an increased amount of certain point defects. The amount and type of these defects have been discussed regarding their influence on device performance.[9]

The abundance of routes for the synthesis of kesterite absorber layers is accompanied by an abundance of challenges and specific obstacles. Together with the importance of general characterisation and profound influence of composition a wide variety of methods is necessary for the investigation of kesterite type materials. This effect is further fueled by the increasing interest in environmentally friendly energy harvesting technologies. In conjunction with X-ray diffraction (XRD) and wavelength dispersive X-ray spectroscopy (WDX), X-ray absorption spectroscopy (XAS) has proven its potential to contribute to the understanding of the fundamental effects of compositional variations on kesterite type materials.[10–13] For example, for the partial or complete replacement of an element like Sn by Ge in $Cu_2Zn(Sn,Ge)Se_4$, extended X-ray absorption fine structure spectroscopy (EXAFS) showed the changes of the local atomic structure with composition.[10] Further studies on technologically relevant thin film samples hinted at several details in the results of alloying that can only be identified with very local structural information.[11] This study, hence, aims to investigate the effects of smaller compositional variations, namely the deviation from stoichiometry, on the atomic scale structure of CZTS, CZTSe and $Cu_2ZnGeSe_4$ (CZGSe) powder samples. Low temperature measurements allow the probing of subtle differences in element specific average bond lengths and their variances depending on the degree of off-stoichiometry. Furthermore, temperature dependent measurements of the basic stoichiometric compounds yield static disorder and the bond stretching force constants for all cation-anion pairs in the three materials. The results are discussed in terms of the local atomic configurations and relevant point defects in these three different kesterite materials.

II. EXPERIMENTAL

Kesterite powder samples from the study by Valle Rios *et al.*[8] based on CZTSe and CZTS, a stoichiometric CZTSe powder sample from Gurieva *et al.*[14] and a stoichiometric CZTS powder sample from Schorr *et al.*[15] were used in this work. Additionally, kesterite powder samples from the study by Gunder *et al.*[16] based on CZGSe as well as a nearly stoichiometric CZGSe by Gurieva *et al.*[17] were analyzed. They were all prepared by solid state reactions with the details described in the respective works. All materials were well characterized with XRD and WDX. The powders chosen for this study are all single phase and exhibit the kesterite crystal structure. Their lattice constants as well as their respective defect types are published in the above studies. The composition of all samples used in this study is shown in Fig. 1 by plotting the Zn/IV ratio vs the Cu/(Zn + IV) ratio which are the two typical cation ratios used to describe the composition of a kesterite type compound. The CZTS and CZTSe samples are all Cu poor and Zn rich and, on average, the Zn/Sn ratio increases with decreasing Cu/(Zn + Sn) ratio.[8] In contrast, the CZGSe samples are both Cu and Zn rich and the Zn/Ge ratio mostly increases with increasing Cu/(Zn + Ge) ratio.[16] From these results it can be concluded, that the local atomic arrangement will be different from the ideal arrangement in a kesterite type structure for less than 4% of the nearest neighbour environments.

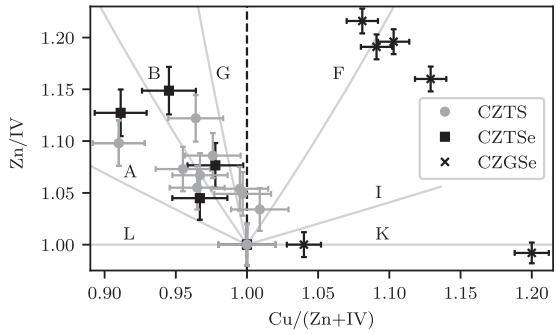

FIG. 1. Cation ratios of the single phase samples from.[8,15,16] Gray lines labeled by capital letters indicate the defect types as described in.[9]

To facilitate EXAFS measurements, the powders were milled in a ball mill together with graphite. This mixture was then pressed into pellets for optimized mechanical stability and handling. The amount of kesterite in the pellet was chosen for optimal signal to noise ratio at each investigated cation absorption edge.

Low temperature EXAFS measurements were performed at beamline BM08 (the LISA beamline) of ESRF.[18,19] The Cu, Zn and Sn cation edge (8979, 9659 and 29 200 eV, respectively) spectra of all CZTS and CZTSe materials discussed in this study were taken in transmission mode. Samples were cooled to 15 ± 1 K by a cold finger liquid helium cryostat with the sample under vacuum conditions. This ensured optimal signal to noise ratio and, hence, highest precision of the measurements.

Low temperature EXAFS measurements of the CZGSe materials and temperature dependent EXAFS measurements of stoichiometric CZTS, CZTSe and CZGSe were conducted at beamline P65 of PETRA III, DESY.[20] Cooling to 15 ± 1 K (low temperature) and to different intermediate temperatures up to room temperature was achieved with a liquid helium flow through cryostat. It has two heating elements at the He inlet and the base of the sample holder and the samples are immersed in the cold He gas. For the CZGSe samples, the Cu, Zn and Ge cation edges (8979, 9659 and 11 103 eV, respectively) were probed at 15 ± 1 K for the same reasons as mentioned above. Additionally, the samples closest to stoichiometry for all three materials as well as the second closest in case of CZTS were measured at all cation edges at 15, 50, 80, 110, 140, 170, 200, 230, 260 and 295 K (room temperature). All spectra were recorded in transmission mode.

In all experiments, elemental metal foils were measured in series with the actual sample to serve as reference for energy alignment. The stoichiometric CZTSe sample was measured at both beamlines at 15 ± 1 K to ensure comparability. For all measurements except those at the Cu K-edge, the k-window for Fourier transformation of the data was 3–15 $Å^{-1}$. For the Cu K-edge, the upper limit had to be set to 12 $Å^{-1}$ due to the Zn K-edge starting slightly beyond this value. The tapering parameter was 2 $Å^{-1}$. Scattering amplitudes and phase shifts were calculated with the FEFF9

software.[21] Fitting of the average bond length (mean value) and the bond length variance (variance of the distance distribution, σ^2) in R-space was carried out with the scripting library LARCH.[22] Higher cummulants (≥3) were tested and identified to be neglectable for the low temperature data and, hence, were set to zero. For the temperature dependent data, at least the third cumulant C3 would have to be included in the fit in order to obtain meaningful bond length values. In this study, however, only the temperature dependence of the variance σ^2 is of interest and the fitting results for it are independent of the inclusion of C3 within the uncertainties, confirming that these amplitude- and phase dependent parameters are not strongly correlated.[23] Therefore, C3 and all higher cumulants were set to zero for the temperature dependent data and only σ^2 was then evaluated as a function of temperature. Final results were based on fits with multiple k-weights (2,3,4).

Uncertainties in this study represent the tested influence of all parameters of data analysis such as the window parameters etc. given above. For the presented data sets, the fitting uncertainty proved dominant. The highest precision was achieved for the CZTSe results.

III. LOCAL CONFIGURATIONS

All of the samples analysed in this study[8,14,16,17,24] adopt the kesterite type structure (space group $I\bar{4}$). It is tetragonal and consists of differently rotated tetrahedra of cations around the anions and vice versa. This basic tetrahedron around an anion is shown for the three analysed kesterites on the left of Fig. 2. As all cations are surrounded by four anions, which in turn are the center of four local configurations as displayed in Fig. 2, any cation is part of four such tetrahedra.

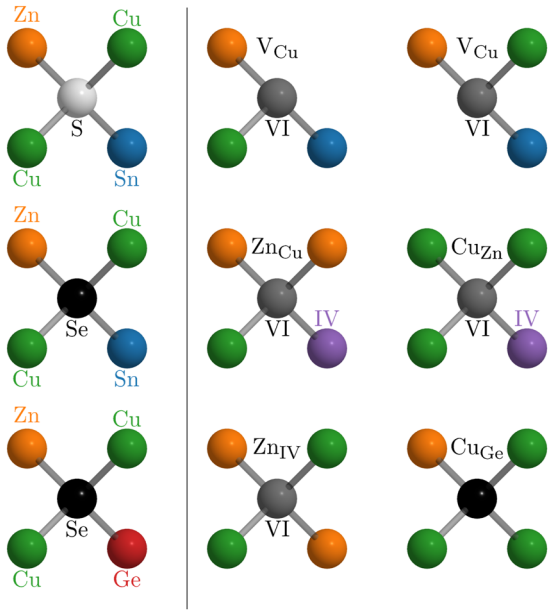

FIG. 2. Left: Local atomic configuration around a central anion for CZTS, CZTSe, CZGSe. Right: Local atomic configurations around a central anion containing a point defect as indicated above each anion.

In all configurations shown on the left of Fig. 2, the stoichiometric ratio of Cu:Zn:Sn = 2:1:1 is kept and, hence, any change in composition resulting in point defects will require additional tetrahedra with different local atomic arrangements. The defects that appear in these materials were determined by analysis of neutron diffraction data and were communicated by the authors of.[8,14,16,17,24] The resulting new configurations are shown on the right of Fig. 2. Whenever any defect is present in different materials, the respective anion or group IV cation is shown as a dark grey or purple placeholder, respectively. The only defects that are not displayed here are interstitials of Zn and Cu. These occur in minor concentrations compared to the other defects[8,14,16,17,24] and will thus influence the local structural parameters on a far less significant scale.

Changing the configuration of cations around an anion will mostly result in a shift of the anion position within the tetrahedron as has been discussed for kesterites[10,11] and other compound semiconductors.[25,26] The qualitative shift of the respective anion in any of the defect configurations can be described by the change of its distance to the cations. As for example the previous results for $Cu_2Zn(Ge,Sn)Se_4$ alloys have shown, the relative anion position shifts mostly along the direction to the defect site.[10] The extent of change in any local configuration is based on the strain resulting from the replacement of a cation with a differently sized species and from the force constants of the individual cation-anion bonds.

With any cation being part of four local atomic configurations, the V_{Cu} defect results in two tetrahedra, each of the two kinds is shown in Fig. 2. Since a vacancy does not create any compressive stress and only relatively weak tensile stress on the remaining bonds, these local configurations will not significantly change the overall bond lengths for the compositional range investigated in this study, as already demonstrated for $Cu(In,Ga)Se_2$ with varying Cu content.[27,28] The next two defects displayed in the middle of Fig. 2 are the Zn_{Cu} and Cu_{Zn} antisites. Note that for Zn_{Cu} two configurations will result as in the case of V_{Cu}. However, they are both just rotated versions of one another and hence only one is shown in Fig. 2. Together, Zn_{Cu} and Cu_{Zn} constitute the well known Cu–Zn disorder.[1,2,9] If both of these defects are within one and the same tetrahedron, the effects will be cancelled out and the resulting tetrahedron will be identical to the standard one with the ideal 2:1:1 ratio. If any of the defects is in an environment of its own, the resulting tetrahedron will be configured as shown in Fig. 2 with either an additional Cu or Zn cation. Zn_{Cu} keeps the degree of symmetry identical to the original tetrahedron, with two identical cations and two types of single cations. Cu_{Zn} as well as Zn_{IV} and Cu_{Ge} remove one type of cation and, hence, change the symmetry. They also only create one possible local configuration each.

While it is not possible to individually probe the local configurations of a defect type, the basic configurations can be studied in the stoichiometric materials. Any deviation in the off-stoichiometric samples must then substantially be due to the combined influence of the respective defect configurations.

IV. FORCE CONSTANTS

The temperature dependent EXAFS measurements on the most stoichiometric samples from CZTS, CZTSe and CZGSe yield the variance of the distance distribution σ^2 as a function of temperature (T) from 15 K to room temperature. The distance distribution

arises from thermal vibrations of the atoms, governed by the stiffness of the respective bond, and from static disorder due to defects or mechanical strain in the material. The temperature dependence can be fitted with an Einstein model in harmonic approximation[29] via the force constant f and a static disorder term σ_s^2:

$$\sigma^2(T) = \frac{\hbar}{2\sqrt{\mu f}} \coth\left(\frac{\hbar}{2k_B T}\sqrt{\frac{f}{\mu}}\right) + \sigma_s^2 \quad (1)$$

Herein μ is the reduced mass of the respective cation-anion pair, $\hbar$ denotes the reduced Planck constant and k_B the Boltzmann constant.

Experimental data of $\sigma^2(T)$ for the Cu–Se bond in CZGSe and the respective fit via Eq. (1) are displayed as an example in Fig. 3. All other kesterite samples and cation-anion pairs showed qualitatively similar behaviour. Data and fit are in excellent agreement and show the increase of σ_s^2 with increasing temperature. The nearly constant value at temperatures below 50 K is larger than the static component σ_s^2 as the thermal contribution does not completely vanish, even at 0 K. Furthermore, it approximately doubles the variance of the distance distribution when reaching room temperature. Low temperatures increase the precision of EXAFS measurements as less thermal movement of the atoms leads to less attenuation of the fine structure and, thus, to a better signal to noise ratio. Consequently, the uncertainties decrease with decreasing temperature and become smaller than the symbol size below 150 K. Hence, they are not visible in this range in Fig. 3. Moreover, the nearly stoichiometric CZGSe sample was measured twice at each temperature and the reproducibility is excellent. Only the two room temperature values show visible differences.

The fit values for both the force constants as well as the static components of all investigated samples can be found in Table I. The force constants are also shown in Fig. 4 to facilitate easier comparison. Results for the two different CZTS based materials only differ within their respective uncertainties. In general and for all materials, the Cu-VI bonds exhibit smaller force constants and hence are softer than the Zn-VI bonds, which in turn are significantly smaller in f than the IV-VI bonds. The latter are thus much stiffer than both the Cu-VI and Zn-VI bonds. These findings

TABLE I. Results of fitting σ^2 as a function of temperature with a harmonic Einstein model [Eq. (1)]. Parameters of the fit were the force constant (f) and a summand (σ_s^2) representing static disorder. CZTS, CZTSe and CZGSe denote the respective samples closest to ideal stoichiometry while CZTS II is characterized by Cu/(Zn + Sn) = 1.01 and Zn/Sn = 1.03.

Material	Pair	f (N/m)	σ_s^2 (10^{-3} Å^2)
CZTS	Cu–S	52 ± 2	0.48 ± 0.08
	Zn–S	86 ± 3	1.0 ± 0.1
	Sn–S	153 ± 10	0.8 ± 0.1
CZTS II	Cu–S	52 ± 2	0.44 ± 0.08
	Zn–S	88 ± 3	1.0 ± 0.1
	Sn–S	155 ± 10	0.8 ± 0.1
CZTSe	Cu–Se	56 ± 2	1.27 ± 0.08
	Zn–Se	80 ± 3	1.3 ± 0.1
	Sn–Se	139 ± 10	0.7 ± 0.1
CZGSe	Cu–Se	58 ± 2	1.32 ± 0.08
	Zn–Se	84 ± 3	0.9 ± 0.1
	Ge–Se	151 ± 4	0.80 ± 0.06

are in good agreement with the general understanding that more ionic bonds are softer than more covalent bonds, as reported in the literature.[26,30] For a given type of bond, e.g. III–VI or II–VI, the force constants also show a small but systematic trend with the constituting elements, namely decreasing for increasing size and hence increasing atomic number.[26] When comparing the different kesterites in Fig. 4, the force constants for a given type of bond are very similar with differences being in the order of the experimental uncertainty in most cases. Nevertheless, considering the IV–VI bond, the f values are similar for Sn–S in CZTS and Ge–Se in CZGSe but higher than the f value for Sn–Se in CZTSe, as expected.[26,30] Similarly, the Zn–S bond in CZTS exhibits a slightly larger force constant than the Zn–Se bond in CZTSe and CZGSe, again as expected. Only the Cu–S bond in CZTS exhibits a slightly lower force constant than the Cu–Se bond in CZTSe and CZGSe contrary to expectation.

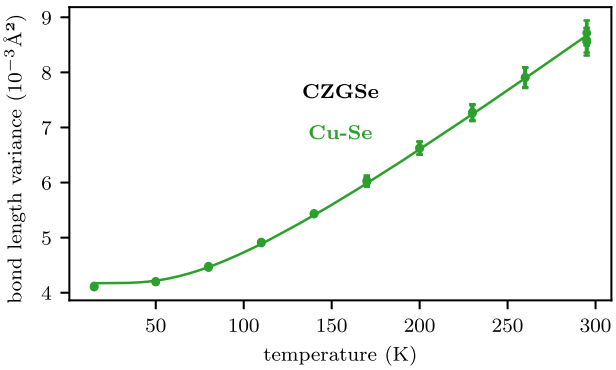

FIG. 3. Variance of the distance distribution σ^2 (bond length variance) as a function of temperature T for the Cu–Se bond in nearly stoichiometric CZGSe. The line represents a fit of the data via Eq. (1).

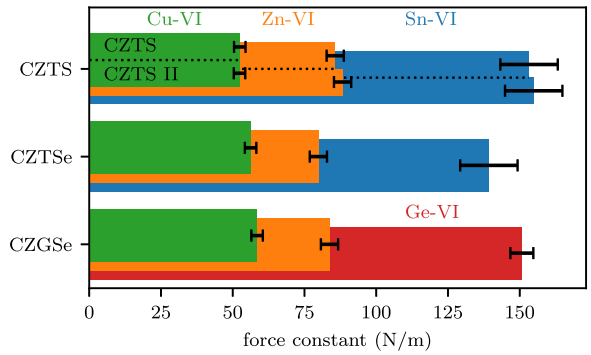

FIG. 4. Force constants from Table I of the CZTS, CZTSe and CZGSe samples closest to ideal stoichiometry while CZTS II is characterized by Cu/(Zn + Sn) = 1.01 and Zn/Sn = 1.03.

Interestingly, the Cu–S bond in both CZTS samples also yields a significantly lower static disorder term than any other bond in Table I. The origin of this unexpected behaviour of the Cu–S bond in CZTS is, however, not clear yet.

V. VARIANCE OF THE DISTANCE DISTRIBUTION

The variance of the distance distribution for all cation-anion bonds in all three types of materials resulting from the low temperature measurements of the off-stoichiometric samples is displayed in Fig. 5. Results are shown as a function of Cu/(Zn + IV) ratio. The following conclusions are also obtained when choosing the (Zn/IV) ratio as the x-axis instead. The mean value of σ^2 is indicated by a dashed line for each cation species in each material. Compared to their uncertainties, there is no clear trend with composition visible in any of the probed types of bonds. Similar findings have been reported for the Cu–Se bond in $Cu(In,Ga)Se_2$ thin films and powders.[28,31] Nevertheless, in these studies the variance of the In–Se and Ga–Se bond lengths increased with decreasing Cu content.[28,31,32] EXAFS studies on CZTS thin films[33] and nanocrystals[34] have shown an effect of disorder on the variance of the distance distribution similar to their uncertainties. Kesterites in an optimal range of the cation ratios exhibit a lower variance of the distance distribution than those in unfavourable areas. The examined range of composition is larger than in the present study and absolute values are higher as the measurements were conducted at significantly higher temperatures. All differences in σ^2 for a given bond in a given material in the present data are within their respective uncertainties, with the exception of Cu–Se and Sn–Se in CZTSe. These two bonds exhibited a significantly higher data quality and, hence, lower uncertainties due to better fits. While they seem to indicate slightly increased values of σ^2 towards ideal stoichiometry [Cu/(Zn + Sn) = 1], there is only a limited data set and the scatter is at least within the same magnitude as the supposed trend. Overall, the deviation from stoichiometry and hence the different types and concentrations of point defects do not have a profound influence on the variance of the element specific bond lengths in the present study.

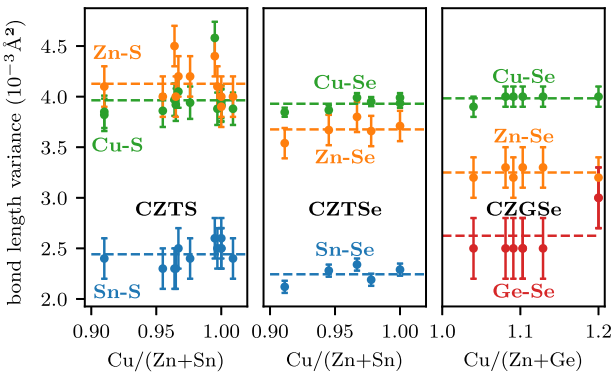

FIG. 5. Variance of the distance distribution σ^2 (bond length variance) for off-stoichiometric CZTS, CZTSe and CZGSe powder samples as a function of the Cu/(Zn + IV) cation ratio. The mean for each material and cation is shown as a dashed line. X-axis errorbars are not shown for clarity here but can be seen in Fig. 1.

However, the differences of σ^2 between the different cation-anion bonds and between CZTS, CZTSe and CZGSe are quite significant (see Fig. 5). Comparing the different cation species, one can see that in any of the three kesterites Cu-VI and Zn-VI are higher in σ^2 than the IV–VI bonds. The comparatively low values for the IV–VI bonds can be understood by the significantly higher force constants presented in Sec. IV (see Table I). The major part of the variance is still due to thermal effects even at low temperature, as can be seen by comparing the static disorder contributions in Table I and the overall variances in Fig. 5. Higher force constants and hence stiffer bonds result in lower variations of the bond length from both thermal vibrations of the atoms and static disorder and thus yield lower σ^2 values. Comparing Zn and Cu, the Zn-VI bond features a higher force constant than the Cu-VI bond in any of the three kesterites. Consequently, the σ^2 values should be lower for Zn-VI than for Cu-VI as indeed observed for CZTSe and CZGSe. The larger difference for CZGSe most probably results from the difference in static disorder for Cu-VI and Zn-VI in this material, whereas the Cu-VI and Zn-VI bonds in CZTSe feature the same static component σ_s^2 within the uncertainty (see Table I). For CZTS, however, the Cu–S values are lower than the Zn–S ones despite the higher Zn–S force constant. This is obviously related to the much lower static disorder term for the Cu–S bond as already discussed in Sec. IV.

Differences in the bond length variance can also be observed when comparing a given cation species for the different kesterite materials (see Fig. 5). For the IV–VI bonds, the CZTSe results are on average slightly lower than those of the other two kesterites, although mostly still within the uncertainties. Since the static disorder contribution is basically identical for the IV–VI bonds in all three materials (see Table I), any differences in σ^2 must arise from the thermal (vibrational) contribution. CZTSe exhibits the lowest IV–VI force constant of the three materials, suggesting a higher thermal contribution in contrast to the experimental results. However, the thermal vibrations are also influenced by the reduced mass of the bond as shown in Eq. (1), leading to decreasing σ^2 for increasing μ. The Sn–Se bond in CZTSe has the highest reduced mass of all IV–VI bonds in this study, resulting in a smaller thermal contribution compared to Sn–S in CZTS and Ge–Se in CZGSe. Similar observations have been made for In–Se and Ga–Se bonds in $Cu(In,Ga)Se_2$,[32] which have similar reduced masses and force constants as Sn–Se and Ge–Se.[35] For the Zn-VI bonds, CZTS exhibits the highest σ^2 values, CZTSe shows intermediate values and CZGSe has the lowest σ^2 (see Fig. 5). The latter two materials, namely CZTSe and CZGSe, both feature a Zn–Se bond with the same reduced mass and comparable force constants (see Table I). Therefore, the thermal contribution to σ^2 is very similar but the static contribution is higher for CZTSe than for CZGSe leading to the observed difference of the overall σ^2 values as already discussed above. The Zn–S bond in CZTS is characterized by a slightly higher force constant and comparable static disorder, but in this case the significantly lower reduced mass compared to the Zn–Se bond results in the highest overall σ^2 values. For the Cu-VI bonds, the variance is the same within the uncertainty for all three materials (see Fig. 5). This agrees well with the expectation for CZTSe and CZGSe as they both feature a Cu–Se bond with the same reduced mass and similar force constants and static disorder terms. For Cu–S of CZTS, however, much higher σ^2 values would be expected based on the significantly lower reduced mass of this bond compared to

Cu–Se. Yet, the much lower static disorder obviously leads to overall σ^2 values comparable to those of the other kesterites.

In summary, the variances of the interatomic distance distributions for the different cation-anion bonds and the different kesterite materials are mostly governed by the bond stretching force constants and reduced masses of these bonds while the deviation from stoichiometry has no notable effect within the studied compositional range.

VI. AVERAGE BOND LENGTH

The *average* bond lengths of all cation-anion bonds in the off-stoichiometric CZTS, CZTSe and CZGSe kesterites resulting from low temperature EXAFS measurements are shown in Fig. 6. Similar to Sec. V, the element specific average bond lengths are displayed as a function of Cu/(Zn + IV) ratio. Changing to the Zn/IV ratio does not affect the conclusions drawn in the following. On the displayed scale, which allows a comparison of all materials and cation species, the uncertainties in average bond length (y-axis) are not visible, as they are smaller than 2×10^{-3} Å. The compositional uncertainties are obtained from the WDX analysis of the samples by Valle Rios *et al.*[8] and Gunder *et al.*[16] Especially for CZTS with the highest number of samples, they create a significant overlap of the data. Overall, none of the element specific average bond lengths of any of the cation species in any of the materials exhibits a clear trend with composition on this scale. A major reason for this are the defect concentrations in the probed kesterites. With one point defect in a volume of several unit cells, their influence on an average measurement like EXAFS is very low.

In all three materials the average Cu-VI bond length is smaller than the average Zn-VI bond length. Furthermore, the average Ge–Se bond length in CZGSe is smaller than Cu–Se by about the same amount. In CZTS and CZTSe, the Sn-VI bonds are larger than the other two bonds by more than twice the difference between Cu-VI and Zn-VI. All these relations are in good agreement with measures of the size of the elements like ionic or covalent radii.[36] With a larger Se anion in CZTSe compared to S in CZTS, all bond lengths are shifted upwards but keep their order. As the lattice has to accommodate the larger anion, it has to expand, which is apparent in the lattice constants as well.[8] The position of the anion, however, is very similar in both materials since the order of the average bond lengths for the three cations is very similar. The same similarities have been shown when replacing S with Se in $CuInS_2$ or $CuGaS_2$.[35] Between CZTSe and CZGSe, there is a significant change in the size of one of the cations which is clearly reflected by the large difference between the average Sn–Se and Ge–Se bond lengths. Again, this results in a corresponding change of the lattice constants.[8,17] The absolute value of the average bond length for Cu–Se and Zn–Se, however, is highly similar in these two materials, resulting in significantly different anion positions as discussed in detail in Ref. 10. The behaviour is qualitatively the same as that reported for the comparison of $CuInSe_2$ and $CuGaSe_2$ or $CuInS_2$ and $CuGaS_2$.[26,35]

As mentioned before, the uncertainties of the data and potential subtle differences between the average bond lengths of the different samples are not visible on this scale. To analyse the data in more detail, the following subsections show the same data on an enlarged scale for each material on its own. To allow a continued comparison of the materials, the absolute range in average bond length (the y-axes interval) is identical for each figure.

A. CZTS

The element specific average bond lengths for CZTS are plotted vs both cation ratios in Fig. 7. There is no trend to be identified as all differences between the different compositions are well within

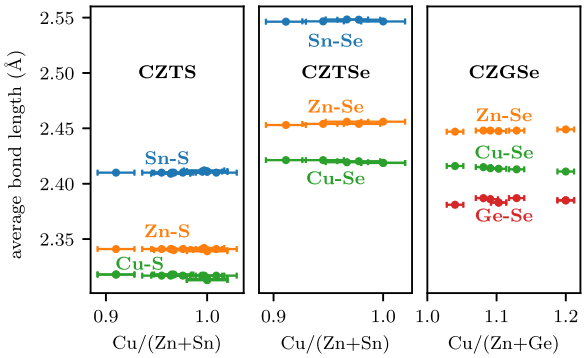

FIG. 6. Element specific average bond lengths for off-stoichiometric CZTS, CZTSe and CZGSe as a function of Cu/(Zn + IV). Y-axis errorbars are about the size of the symbols and are therefore not visible.

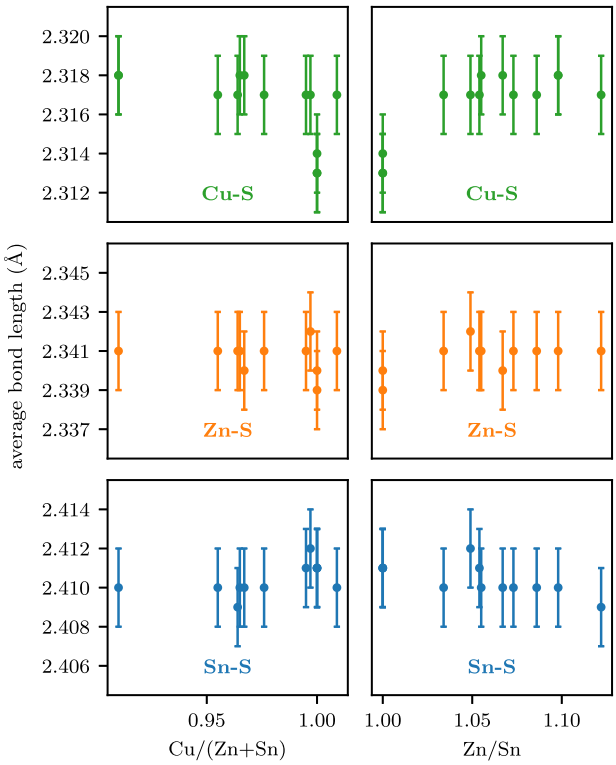

FIG. 7. Element specific average bond lengths for off-stoichiometric CZTS as a function of Cu/(Zn + Sn) (left column) and Zn/Sn (right column). X-axis uncertainties are not displayed for clarity.

the uncertainties. The only clear exception to this is the stoichiometric sample at Zn/Sn=Cu/(Zn + Sn) = 1. It has a significantly lower Cu–S average bond length and a slightly lower Zn–S average bond length. The two data points at the same composition indicate two separate measurements, highlighting the excellent reproducibility. This shows that the different bond lengths in the stoichiometric sample are not an artefact of the single measurement. Instead this sample was from another study with significantly longer annealing times and smaller lattice constants.[15] The fact that the Cu–S bond is affected the most and the Sn–S bond shows no significant difference can result from the higher bond stretching force constant of the Sn–S bond compared to the Cu–S bond as discussed above (see Table I). Nevertheless, all average bond lengths are in good agreement with previously published EXAFS results for CZTS.[33,37,38]

B. CZTSe

Figure 8 displays the element specific average bond lengths from the low temperature measurements for the CZTSe samples as a function of both cation ratios. On this scale, one can clearly see that the uncertainty is significantly smaller than for the CZTS samples. This is mostly due to the heavier Se creating a stronger fine structure than the lighter S. While the differences in average bond lengths are only slightly smaller than for CZTS, they are mostly significant against the lower uncertainty, especially for the Cu–Se bond. The average bond lengths for stoichiometric CZTSe are in good agreement with EXAFS results found in literature.[10–12]

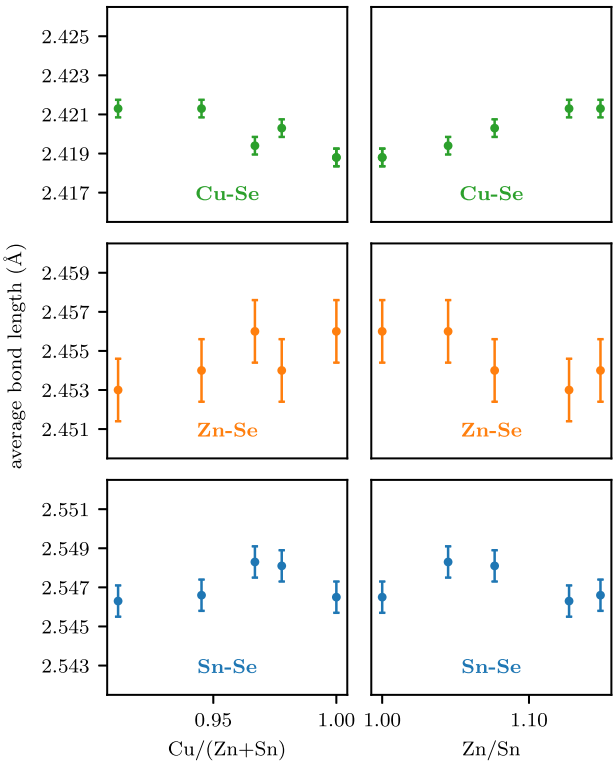

FIG. 8. Element specific average bond lengths for off-stoichiometric CZTSe as a function of Cu/(Zn + Sn) (left column) and Zn/Sn (right column). X-axis uncertainties are not displayed for clarity.

For the five investigated samples, an increase of the average Cu–Se bond length with increasing Zn/Sn ratio is evident. Although slightly less clear, the trend is also visible as a decrease with increasing Cu/(Zn + Sn). This is due to an anti-correlation of Zn/Sn and Cu/(Zn + Sn) in the CZTSe samples (see Fig. 1). Zn–Se exhibits the largest uncertainties of the three bonds but a slight decrease of the average bond length with increasing Zn/Sn can still be perceived. As a function of Cu/(Zn + Sn), the samples at higher values alternate in their bond lengths and any perceived trend upwards is only based on the value of the most off-stoichiometric sample. Nevertheless, the direction of these trends is the same as that reported for CZTS nanocystals.[34] In the Sn–Se bond lengths, no clear trend with any of the cation ratios is evident.

The prior defect analysis, based on neutron diffraction studies, reported the typical Cu–Zn disorder with an increasing excess of Zn_{Cu} defects as well as an increase of Zn_{Sn} defects with increasing off-stoichiometry (decreasing Cu/(Zn + Sn) and increasing Zn/Sn) of these CZTSe samples. While two samples did show V_{Cu} defects, these are not expected to influence the bond lengths, as discussed in Sec. III. Local atomic arrangements for all the mentioned defects are displayed in Fig. 2. Table II summarizes the influence of each of the point defects on the respective cation-anion bonds. An upwards arrow indicates an elongation of a bond, while a downwards arrow indicates a compression, both in relation to the ideal configuration of two Cu, one Zn and one Sn around the central Se. The impact of a defect on the surrounding bonds can be deduced from the average bond lengths as shown in Fig. 6. The average Zn–Se bond length is larger than the average Cu–Se bond lengths. Therefore, Zn_{Cu} induces compressive strain on all surrounding bonds. In contrast, Cu_{Zn} and Zn_{Sn} induce a stretching of all bonds because the average bond length is smaller for Cu–Se compared to Zn–Se and for Zn–Se compared to Sn–Se. Furthermore, EXAFS measurements average over all instances of an element in the analyzed sample. Therefore, the number of arrows indicates the number of the affected bonds within the defect configuration as a weighting factor for this average. In absolute terms, the change in bond lengths will depend on the difference in bond length between the original and the replacing element and on the force constants of each individual bond (see Sec. IV). Since the Zn–Se bond is slightly stiffer than the Cu–Se bond, it will respond somewhat less to the compressive or tensile strain induced by replacing one element with a different one. Similarly, the Sn–Se bond will be much less affected than the Cu–Se and Zn–Se bonds due to its higher force constant.

TABLE II. Qualitative influence of each defect on each cations average bond length to the anion in CZTSe. An ⇑ indicates a stretching of the bond, a ⇓ a compression and a - indicates no influence. The number of arrows indicates the number of the respective type of bond in the defects local configuration as shown in Fig. 2.

Defect	Cu	Zn	Sn
Zn_{Cu}	⇓	⇓⇓	⇓
Cu_{Zn}	⇑⇑⇑	· · ·	⇑
Zn_{Sn}	⇑⇑	⇑⇑	· · ·
V_{Cu}	· · ·	· · ·	· · ·

Regarding the average Sn–Se bond length, only two of the defect types introduce strain on the Sn–Se bonds, namely Zn_{Cu} and Cu_{Zn}, and these have opposing effects. With increasing deviation from the ideal stoichiometry [decreasing Cu/(Zn + Sn) and increasing Zn/Sn], Zn_{Cu} exists in increasing excess compared to Cu_{Zn}, which causes a surplus of shorter Sn–Se bonds. Nevertheless, their influence on the average Sn–Se bond length is limited by the low amount of defects compared to the total number of atoms, by the stiffness of the Sn–Se bond and by the fact that for each defect only one Sn–Se bond is present in the corresponding local environment. As a result, there is no conclusive trend expected or observed with composition.

Zn–Se bonds are present in the local environments of both Zn_{Cu} and Zn_{Sn}, where they are compressed and stretched respectively. For each of the two defects, there are two Zn–Se bonds in the corresponding local configuration. The difference in bond length and, hence, the strain on the local environment is much higher when replacing Sn by Zn as compared to replacing Cu by Zn. Therefore, the resulting change of the bond lengths is expected to be larger for Zn_{Sn} than for Zn_{Cu}. However, the defect concentrations were found to include about two to five times more excess Zn_{Cu} than Zn_{Sn}. Since here only the Zn_{Cu} defects in excess of Cu_{Zn} defects are regarded, their effect on the average Zn–Se bond length cannot be cancelled by Cu_{Zn} defects in the same local configurations (Cu–Zn disorder) as discussed in Sec. III. Thus, if any change of the average Zn–Se bond length occurs at all, a small decrease with increasing Zn/Sn ratio is expected due to the much larger Zn_{Cu} concentration compared to Zn_{Sn}, which is in good qualitative agreement with the results shown in Fig. 8.

Cu–Se is the softest bond in CZTSe and is influenced by all three relevant defects present in the given sample set. With two Cu cations in the standard CZTSe configuration, this number rises to three when adding an extra Cu instead of Zn in Cu_{Zn} and is reduced to one when replacing one of the two Cu with Zn in Zn_{Cu}. The two defects with the higher amounts of Cu–Se bonds both contribute longer Cu–Se bond lengths to the overall average while Zn_{Cu} contributes shorter than average Cu–Se bond lengths. As discussed above, Cu_{Zn} and Zn_{Cu} within the same tetrahedron do not lead to a change in bond lengths. However, even for the Cu–Zn disorder, some Cu_{Zn} and Zn_{Cu} defect configurations as shown in Fig. 2 will remain. Despite the excess of Zn_{Cu}, the longer bond lengths of Cu_{Zn} and Zn_{Sn} result in an overall increase of the average Cu–Se bond length with increasing degree of off-stoichiometry as seen in Fig. 8.

C. CZGSe

The CZGSe samples are in a different region of off-stoichiometry, being both Zn and Cu rich.[16] In these samples, higher Cu/(Zn + Ge) ratios typically correspond to lower Zn/Ge ratios (see Fig. 1). The element specific average bond lengths for CZGSe on the enlarged scale can be seen in Fig. 9. No clear trend as function of either cation ratio is observed for the Zn–Se or Ge–Se average bond lengths. The uncertainties for these two bonds are similar to those for the CZTS data, however the spread of the Ge–Se bond length is larger than that of Sn–S or that of Sn–Se in CZTSe, but still without any systematic correlation to the sample composition. In contrast the Cu–Se bond length exhibits a distinctive decrease with increasing

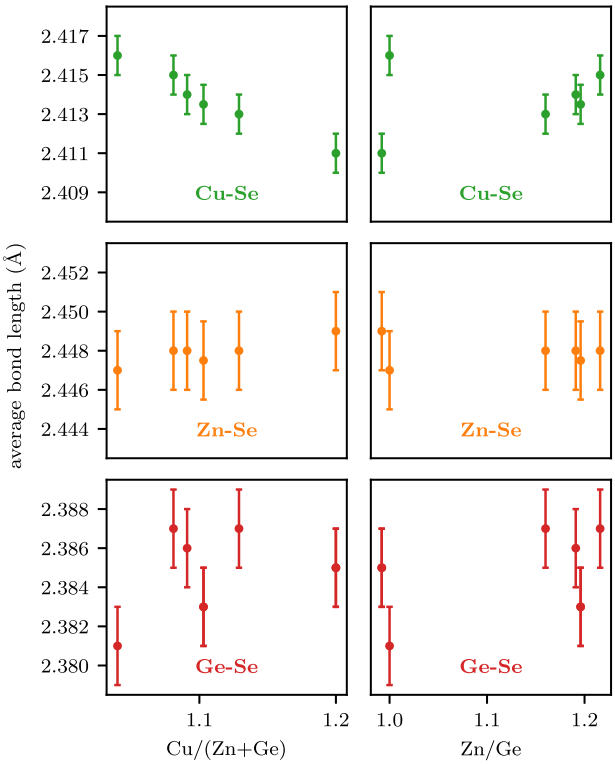

FIG. 9. Element specific average bond lengths for off-stoichiometric CZGSe as a function of Cu/(Zn + Ge) (left column) and Zn/Ge (right column). X-axis uncertainties are not displayed for clarity.

Cu/(Zn + Ge). Except for the sample closest to the ideal stoichiometric ratios of Zn/Ge = 1 and Cu/(Zn + Ge) = 1, this corresponds to an increase of the average Cu–Se bond length with increasing Zn/Ge. However, the difference between the two samples with Zn/Ge ~ 1 yet Cu/(Zn + Ge) of 1.04 and 1.20 clearly shows that in this case the Cu content is the decisive compositional property. The absolute change in average Cu–Se bond length is nearly twice that for CZTSe and as the change in Cu/(Zn + IV) is also nearly twice that of CZTSe, their slopes are similar. Nevertheless, the CZGSe sample also exhibit about twice as high uncertainties for the individual average bond length values.

Besides the Cu–Zn disorder, mostly Cu_{Ge} and Zn_{Ge} defects were reported for these samples. Ge is significantly smaller than Sn, as evident from the Ge–Se and Sn–Se bond lengths in CZGSe and CZTSe, respectively (see Fig. 6). The Ge–Se bond length is even smaller than the Cu–Se and Zn–Se bond lengths. Nevertheless, the stiffness of Ge–Se is even higher than that of Sn–Se, which is clear from their respective force constants shown in Table I. The number of bonds resulting for the different defect configurations and their length change relative to the configuration without point defects is presented in Table III. The difference between Zn–Se and Cu–Se average bond lengths is similar in CZGSe and CZTSe, hence, all arguments about the qualitative changes for Zn_{Cu} and Cu_{Zn} are the same as for CZTSe (see Table II). In contrast to Zn_{Sn}, however,

TABLE III. Qualitative influence of each defect on each cations average bond length to the anion in CZGSe. An ⇑ indicates a stretching of the bond, a ⇓ a compression and a - indicates no influence. The number of arrows indicates the number of the respective type of bond in the defects local configuration as shown in Fig. 2.

Defect	Cu	Zn	Ge
Zn_{Cu}	⇓	⇓⇓	⇓
Cu_{Zn}	⇑⇑⇑	···	⇑
Zn_{Ge}	⇓⇓	⇓⇓	···
Cu_{Ge}	⇓⇓⇓	⇓	···

replacement of Ge by either Zn or Cu leads to a compression of all surrounding bonds due to the size differences discussed above.

For the Ge–Se bonds, the changes caused by the Cu–Zn disorder defects cancel if they are part of the same local configuration or still counteract each other if they are not part of the same tetrahedron as discussed above for CZTSe. Therefore, no change of the average Ge–Se bond length is expected for similar concentrations of Zn_{Cu} and Cu_{Zn}. Only the sample with Zn/Ge < 1 and Cu/(Zn + Ge) = 1.20 features an excess of one of these two defects with nearly twice as many Cu_{Zn} as Zn_{Cu}. Nevertheless, the Ge–Se bond length of this sample is still well within the spread of the data, probably because the very stiff Ge–Se bonds do not change much even in the defect configurations, similar to what was observed for the Sn–Se bonds in CZTSe.

Zn–Se as the longest bond in CZGSe is compressed in any of the local configurations with a point defect, however, it still does not exhibit any trend with changing stoichiometry. A possible reason for the behaviour could be that the total concentration of all point defects together is similar for all samples, even the one closest to the ideal stoichiometry, and that the combined impact of these defects on the average Zn–Se bond lengths is thus similar for all studied samples.

Cu–Se bonds are present in the local configurations of all point defects reported for this material. Cu_{Zn} defects with the highest concentration and three elongated Cu–Se bonds are counteracted by all other defects, which contain one to three compressed Cu–Se bonds. The overall result in this case is the decrease of the average Cu–Se bond length with increasing Cu/(Zn + Ge) seen in Fig. 9.

VII. CONCLUSIONS

Element specific bond stretching force constants of stoichiometric CZTS and CZTSe and nearly stoichiometric CZGSe powder samples were determined by temperature dependent EXAFS measurements. The Cu-VI bond exhibits the smallest force constant and is thus the softest bond in any of the three materials. The Zn-VI bond has a slightly higher force constant and is thus somewhat stiffer while the IV–VI bond features a much higher force constant and is thus by far the stiffest bond in all three materials. This agrees very well with the known fact that bonds become softer with increasing ionicity and stiffer with increasing covalent character. Subtle differences in the force constants between the different kesterite materials match the trend of decreasing bond stiffness with increasing size and hence atomic number of the constituent elements. The only exception to this known behaviour in the present study is the Cu–S bond in CZTS, which exhibits an unexpectedly low force constant as well as the lowest static disorder of all bonds and materials.

The variances of the element specific bond length distributions and their average values were determined for series of off-stoichiometric CZTS, CZTSe and CZGSe powder samples by low temperature EXAFS measurements. The bond length distribution arises from thermal atomic vibrations that are present even at low temperature and from static disorder originating from defects or strain in the material. The variance of the bond length distribution does not show significant trends with composition for any of the cation-anion bonds. For IV–VI, the variance is much lower than for Zn-VI and Cu-VI due to the higher force constants of the IV–VI bonds. For Zn-VI and Cu-VI, the force constants are more similar, such that the actual differences observed for the variance are also governed by static disorder contributions. Subtle differences in the variances between the different kesterite materials can further be explained by the influence of the reduced mass of the cation anion pair. In summary, the variances of the bond length distributions are mostly governed by the bond stretching force constants and reduced masses of the bonds while the off-stoichiometry has no notable effect within the studied compositional range.

Significant differences are observed for the element specific average bond lengths. Cu–S is the shortest bond in CZTS, followed by Zn–S and with a larger difference by Sn–S as the longest bond. The same sequence is found for CZTSe, only with bond lengths shifted to higher values due to the larger Se anion. Zn–Se and Cu–Se bond lengths are nearly identical in CZGSe and CZTSe, yet, Ge–Se is the shortest bond in CZGSe. All these findings are in excellent agreement with previous studies of kesterites and similar materials. On a scale where the uncertainties of the derived element specific average bond lengths become relevant, CZTS does not show any relevant trends of the bond lengths with composition, except for the nearly stoichiometric sample, which was prepared under different experimental conditions. In CZTSe, the Cu–Se bond length shows a substantial trend with composition, the Zn–Se bond length still shows a noticeable but less pronounced trend and the Sn–Se bond does not exhibit any systematic dependence in the analysed compositional range. This is in good agreement with the defect types and concentrations in these samples and with the expected changes of the bond lengths in the defect environment. The latter are governed by the size mismatch of the elements and by the force constants of their bonds. Given the significant changes of bond length and the low number of defects compared to the number of atoms, this clearly shows that the bond lengths around point defects must significantly differ from those of the defect free configurations in order for them to influence the averaging EXAFS results. This obviously needs to be taken into account for precise theoretical modelling of the electronic and optical material properties of kesterites. For CZGSe, only the Cu–Se bond length shows a trend, which is significant compared to the uncertainties, resulting from the combined effect of different defect environments on the average value of the bond length distribution.

In summary, the present study has investigated different properties of the element specific atomic scale structure of stoichiometric and off-stoichiometric CZTS, CZTSe and CZGSe kesterites. Some of these structural parameters are found to change with changing composition while others do not. As known for many

compound semiconductors, including chalcopyrites and kesterites, these local structural parameters affect other important material properties.[10,11,26] Understanding and controlling all influences caused by off-stoichiometry is therefore key to improving the application and efficiency of kesterite type solar cell materials.

ACKNOWLEDGMENTS

The authors thank Laura Elisa, Valle Rios, and Kai Neldner for the synthesis of the different kesterite materials and their characterization by WDX and XRD. We acknowledge the ESRF and the CNR-IOM for provision of synchrotron radiation facilities (experiment: HC-2412) and we thank Alessandro Puri, Philipp Schöppe, and Robert Röder for their valuable help during the beamtime at LISA (Grant No. BM08). We further acknowledge DESY (Hamburg, Germany), a member of the Helmholtz Association HGF, for the provision of experimental facilities. Parts of this research were carried out at beamline P65 of PETRA III under proposals Grant Nos. I-20160075 and II-20200005 and we thank Roman Chernikov, Morgane Desmau, Hans H. Falk, Timo Pfeiffelmann, and Sergiu Levcenko for their valuable support during the beamtimes. This work was funded (without any involvement in the conduct of the research) by the Deutsche Forschungsgemeinschaft (DFG, German Research Foundation) under project Grant No. SCHN 1283/2-1.

AUTHOR DECLARATIONS

Conflict of Interest

The authors have no conflicts to disclose.

Author Contributions

Konrad Ritter: Data curation (lead); Formal analysis (lead); Investigation (equal); Methodology (equal); Software (lead); Visualization (lead); Writing – original draft (lead); Writing – review & editing (equal). **Galina Gurieva**: Resources (equal); Writing – review & editing (equal). **Stefanie Eckner**: Investigation (equal); Methodology (equal); Writing – review & editing (equal). **Rene Schwiddessen**: Resources (equal); Writing – review & editing (equal). **Francesco d'Acapito**: Investigation (equal); Resources (equal); Writing – review & editing (equal). **Edmund Welter**: Investigation (equal); Resources (equal); Writing – review & editing (equal). **Susan Schorr**: Resources (equal); Writing – review & editing (equal). **Claudia S. Schnohr**: Conceptualization (lead); Funding acquisition (lead); Investigation (equal); Methodology (equal); Project administration (lead); Supervision (lead); Writing – review & editing (equal).

DATA AVAILABILITY

The data that support the findings of this study are available from the corresponding author upon reasonable request.

REFERENCES

[1] S. Giraldo, Z. Jehl, M. Placidi, V. Izquierdo-Roca, A. Pérez-Rodríguez, and E. Saucedo, "Progress and perspectives of thin film kesterite photovoltaic technology: A critical review," Adv. Mater. **31**, 1806692 (2019).

[2] A. S. Nazligul, M. Wang, and K. L. Choy, "Recent development in earth-abundant kesterite materials and their applications," Sustainability **12**, 5138 (2020).

[3] T. E. E. Communication From The Commission To The European Parliament, The Council, S. Committee, and T. C. O. T. Regions, Critical raw materials resilience: Charting a path towards greater security and sustainability com/2020/474 final, 2020.

[4] L. H. Wong, A. Zakutayev, J. D. Major, X. Hao, A. Walsh, T. K. Todorov, and E. Saucedo, "Emerging inorganic solar cell efficiency tables (version 1)," J. Phys.: Energy **1**, 032001 (2019).

[5] J. Zhou, X. Xu, B. Duan, H. Wu, J. Shi, Y. Luo, D. Li, and Q. Meng, "Regulating crystal growth via organic lithium salt additive for efficient kesterite solar cells," Nano Energy **89**, 106405 (2021).

[6] D.-H. Son, S.-H. Kim, S.-Y. Kim, Y.-I. Kim, J.-H. Sim, S.-N. Park, D.-H. Jeon, D.-K. Hwang, S.-J. Sung, J.-K. Kang, K.-J. Yang, and D.-H. Kim, "Effect of solid-H_2S gas reactions on CZTSSe thin film growth and photovoltaic properties of a 12.62% efficiency device," J. Mater. Chem. A **7**, 25279–25289 (2019).

[7] W. Shockley and H. J. Queisser, "Detailed balance limit of efficiency of p-n junction solar cells," J. Appl. Phys. **32**, 510–519 (1961).

[8] L. E. Valle Rios, K. Neldner, G. Gurieva, and S. Schorr, "Existence of off-stoichiometric single phase kesterite," J. Alloys Compd. **657**, 408–413 (2016).

[9] S. Schorr, G. Gurieva, M. Guc, M. Dimitrievska, A. Pérez-Rodríguez, V. Izquierdo-Roca, C. S. Schnohr, J. Kim, W. Jo, and J. M. Merino, "Point defects, compositional fluctuations, and secondary phases in non-stoichiometric kesterites," J. Phys.: Energy **2**, 012002 (2019).

[10] K. Ritter, S. Eckner, C. Preiß, G. Gurieva, T. Bischoff, E. Welter, S. Botti, S. Schorr, and C. S. Schnohr, "Atomic scale structure and its impact on the band gap energy for $Cu_2Zn(Sn,Ge)Se_4$ kesterite alloys," J. Phys.: Energy **2**, 035004 (2020).

[11] K. Ritter, G. Gurieva, S. Eckner, C. Preiß, M. Ritzer, C. J. Hages, E. Welter, R. Agrawal, S. Schorr, and C. S. Schnohr, "Atomic scale structure of $(Ag,Cu)_2ZnSnSe_4$ and $Cu_2Zn(Sn,Ge)Se_4$ kesterite thin films," Front. Energy Res. **9**, 656006 (2021).

[12] S. Quadir, M. Qorbani, A. Sabbah, T.-S. Wu, A. k. Anbalagan, W.-T. Chen, S. M. Valiyaveettil, H.-T. Thong, C.-W. Wang, C.-Y. Chen, C.-H. Lee, K.-H. Chen, and L.-C. Chen, "Short- and long-range cation disorder in $(Ag_xCu_{1-x})_xZnSnSe_4$ kesterites," Chem. Mater. **34**, 7058–7068 (2022).

[13] M. J. Turnbull, Y. M. Yiu, M. Goldman, T.-K. Sham, and Z. Ding, "Favorable bonding and band structures of Cu_2ZnSnS_4 and CdS films and their photovoltaic interfaces," ACS Appl. Mater. Interfaces **14**, 32683–32695 (2022).

[14] G. Gurieva, D. M. Többens, S. Levcenco, T. Unold, and S. Schorr, "Cu/Zn disorder in stoichiometric $Cu_2ZnSn(S_{1-x}Se_x)_4$ semiconductors: A complementary neutron and anomalous X-ray diffraction study," J. Alloys Compd. **846**, 156304 (2020).

[15] S. Schorr, H.-J. Hoebler, and M. Tovar, "A neutron diffraction study of the stannite-kesterite solid solution series," Eur. J. Mineral. **19**, 65–73 (2007).

[16] R. Gunder, J. A. Márquez-Prieto, G. Gurieva, T. Unold, and S. Schorr, "Structural characterization of off-stoichiometric kesterite-type $Cu_2ZnGeSe_4$ compound semiconductors: From cation distribution to intrinsic point defect density," CrystEngComm **20**, 1491–1498 (2018).

[17] G. Gurieva, D. Többens, M. Y. Valakh, and S. Schorr, "Cu-Zn disorder in $Cu_2ZnGeSe_4$: A complementary neutron diffraction and Raman spectroscopy study," J. Phys. Chem. Solids **99**, 100–104 (2016).

[18] F. d'Acapito, A. Trapananti, and A. Puri, "LISA: The Italian CRG beamline for x-ray absorption spectroscopy at ESRF," J. Phys.: Conf. Ser. **712**, 012021 (2016).

[19] F. d'Acapito, G. O. Lepore, A. Puri, A. Laloni, F. La Manna, E. Dettona, A. De Luisa, and A. Martin, "The LISA beamline at ESRF," J. Synchrotron Radiat. **26**, 551–558 (2019).

[20] E. Welter, R. Chernikov, M. Herrmann, and R. Nemausat, "A beamline for bulk sample x-ray absorption spectroscopy at the high brilliance storage ring PETRA III," AIP Conf. Proc. **2054**, 040002 (2019).

[21] J. J. Rehr, J. J. Kas, F. D. Vila, M. P. Prange, and K. Jorissen, "Parameter-free calculations of X-ray spectra with FEFF9," Phys. Chem. Chem. Phys. **12**, 5503 (2010).

[22]M. Newville, "Larch: An analysis package for XAFS and related spectroscopies," J. Phys.: Conf. Ser. **430**, 012007 (2013).
[23]C. S. Schnohr, P. Kluth, L. L. Araujo, D. J. Sprouster, A. P. Byrne, G. J. Foran, and M. C. Ridgway, "Anisotropic vibrations in crystalline and amorphous InP," Phys. Rev. B **79**, 195203 (2009).
[24]G. Gurieva, L. E. V. Rios, A. Franz, P. Whitfield, and S. Schorr, "Intrinsic point defects in off-stoichiometric $Cu_2ZnSnSe_4$: A neutron diffraction study," J. Appl. Phys. **123**, 161519 (2018).
[25]A. Balzarotti, N. Motta, A. Kisiel, M. Zimnal-Starnawska, M. T. Czyyk, and M. Podgórny, "Model of the local structure of random ternary alloys: Experiment versus theory," Phys. Rev. B **31**, 7526–7539 (1985).
[26]C. S. Schnohr, "Compound semiconductor alloys: From atomic-scale structure to bandgap bowing," Appl. Phys. Rev. **2**, 031304 (2015).
[27]C. S. Schnohr, H. Kämmer, C. Stephan, S. Schorr, T. Steinbach, and J. Rensberg, "Atomic-scale structure and band-gap bowing in $Cu(In,Ga)Se_2$," Phys. Rev. B **85**, 245204 (2012).
[28]E. Haubold, P. Schöppe, S. Eckner, S. Lehmann, I. Colantoni, F. d'Acapito, F. di Benedetto, S. Schorr, and C. S. Schnohr, "Short-range versus long-range structure in $Cu(In,Ga)Se_2$, $Cu(In,Ga)_3Se_5$, and $Cu(In,Ga)_5Se_8$," J. Alloys Compd. **774**, 803–812 (2019).
[29]P. Fornasini, "Study of lattice dynamics via extended x-ray absorption fine structure," J. Phys.: Condens. Matter **13**, 7859–7872 (2001).
[30]S. Eckner, A. Johannes, M. Gnauck, H. Kämmer, T. Steinbach, S. Schönherr, R. Chernikov, E. Welter, M. C. Ridgway, and C. S. Schnohr, "Bond-stretching force constants and vibrational frequencies in ternary zinc-blende alloys: A systematic comparison of (In,Ga)P, (In,Ga)As and Zn(Se,Te)," EPL (Europhys. Lett.) **126**, 36002 (2019).
[31]C. Schnohr, H. Kämmer, T. Steinbach, M. Gnauck, T. Rissom, C. Kaufmann, C. Stephan, and S. Schorr, "Composition-dependent nanostructure of $Cu(In,Ga)Se_2$ powders and thin films," Thin Solid Films **582**, 356–360 (2015).
[32]C. S. Schnohr, S. Eckner, P. Schöppe, E. Haubold, F. d'Acapito, D. Greiner, and C. A. Kaufmann, "Reversible correlation between subnanoscale structure and Cu content in co-evaporated $Cu(In,Ga)Se_2$ thin films," Acta Mater. **153**, 8–14 (2018).
[33]R. Colina-Ruiz, J. M. de León, J. Lezama-Pacheco, F. Caballero-Briones, M. Acosta-Alejandro, and F. Espinosa-Faller, "Local atomic structure and analysis of secondary phases in non-stoichiometric Cu_2ZnSnS_4 using X-ray absorption fine structure spectroscopy," J. Alloys Compd. **714**, 381–389 (2017).
[34]M. J. Turnbull, S. Khoshmashrab, Y. M. Yiu, and Z. Ding, "Resolving the effects of compositional change on structures in Cu_2ZnSnS_4 nanocrystals by X-ray absorption fine structure," Can. J. Chem. **96**, 785–794 (2018).
[35]S. Eckner, H. Kämmer, T. Steinbach, M. Gnauck, A. Johannes, C. Stephan, S. Schorr, and C. S. Schnohr, "Atomic-scale structure, cation distribution, and bandgap bowing in $Cu(In,Ga)S_2$ and $Cu(In,Ga)Se_2$," Appl. Phys. Lett. **103**, 081905 (2013).
[36]R. D. Shannon, "Revised effective ionic radii and systematic studies of interatomic distances in halides and chalcogenides," Acta Crystallogr., Sect. A **32**, 751–767 (1976).
[37]R. Bacewicz, J. Antonowicz, S. Podsiadło, and S. Schorr, "Local structure in Cu_2ZnSnS_4 studied by the XAFS method," Solid State Commun. **177**, 54–56 (2014).
[38]F. J. Espinosa-Faller, D. R. Conradson, S. C. Riha, M. B. Martucci, S. J. Fredrick, S. Vogel, A. L. Prieto, and S. D. Conradson, "Neutron diffraction and x-ray absorption fine structure evidence for local lattice distortions and aperiodic antisite substitution in Cu_2ZnSnS_4 nanoparticles," J. Phys. Chem. C **118**, 26292–26303 (2014).